© American Society for Mass Spectrometry, 2019

J. Am. Soc. Mass Spectrom. (2019) 30:1758–1767
DOI: 10.1007/s13361-019-02274-8

RESEARCH ARTICLE

Impact of Sodium Cationization on Gas-Phase Conformations of DNA and RNA Cytidine Mononucleotides

L. A. Hamlow,[1] Y.-w. Nei,[1] R. R. Wu,[1] J. Gao,[2] J. D. Steill,[2] G. Berden,[2] J. Oomens,[2] M. T. Rodgers[1]

[1]Department of Chemistry, Wayne State University, 5101 Cass Ave, Detroit, MI 48202, USA
[2]Institute for Molecules and Materials, FELIX Laboratory, Radboud University, Toernooiveld 7c, 6525 ED, Nijmegen, Netherlands

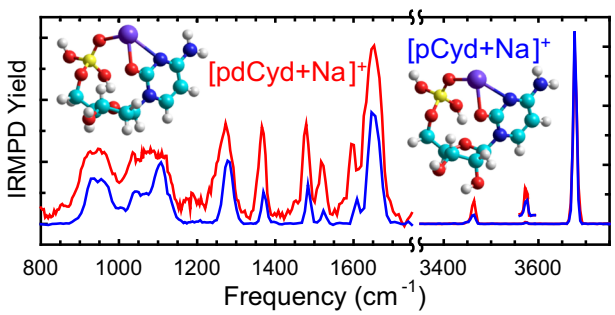

Abstract. Gas-phase conformations of the sodium-cationized forms of the 2′-deoxycytidine and cytidine mononucleotides, $[pdCyd+Na]^+$ and $[pCyd+Na]^+$, are examined by infrared multiple photon dissociation action spectroscopy. Complimentary electronic structure calculations at the B3LYP/6-311+G(2d,2p)//B3LYP/6-311+G(d,p) level of theory provide candidate conformations and their respective predicted IR spectra for comparison across the IR fingerprint and hydrogen-stretching regions. Comparisons of the predicted IR spectra and the measured infrared multiple photon dissociation action spectra provide insight into the impact of sodium cationization on intrinsic mononucleotide structure. Further, comparison of present results with those reported for the sodium-cationized cytidine nucleoside analogues elucidates the impact of the phosphate moiety on gas-phase structure. Across the neutral, protonated, and sodium-cationized cytidine mononucleotides, a preference for stabilization of the phosphate moiety and nucleobase orientation is observed, although the details of this stabilization differ with the state of cationization. Several low-energy conformations of $[pdCyd+Na]^+$ and $[pCyd+Na]^+$ involving several different orientations of the phosphate moiety and sugar puckering modes are observed experimentally.

Keywords: Cytidine (Cyd), Cytidine-5′-monophosphate (pCyd), Density functional theory (DFT), 2′-Deoxycytidine (dCyd) , 2′-Deoxycytidine-5′-monophosphate (pdCyd), Electronic structure calculations, Electrospray ionization (ESI), Fourier transform ion cyclotron resonance mass spectrometer (FT-ICR MS), Gas-phase conformation, Hydrogen-bonding interactions, Hydrogen-stretching region, Infrared multiple photon dissociation (IRMPD) action spectroscopy, IR fingerprint region, IRMPD spectrum, IR spectrum, Mononucleotide, Nucleobase, Nucleobase orientation, Nucleoside, Phosphate moiety, Protonation, Quadrupole ion trap mass spectrometer (QIT MS), Simulated annealing, Sodium cationization, Sugar puckering, Tandem mass spectrometry

Received: 14 May 2019/Revised: 18 June 2019/Accepted: 20 June 2019/Published Online: 8 July 2019

Introduction

The alkali metal cations Na^+ and K^+ are well known to play a variety of critical roles in biology [1, 2]. The alkali metal cations are often dependent on one another to create electrical potentials between environments to drive a specific action, such as driving the flow of water through a membrane [3, 4]. In addition, the structure and function of DNA and RNA nucleic acids is often influenced by the presence of metal ions

Electronic supplementary material The online version of this article (https://doi.org/10.1007/s13361-019-02274-8) contains supplementary material, which is available to authorized users.

Correspondence to: M. T. Rodgers; *e-mail:* mrodgers@chem.wayne.edu

[5]. However, the ion atmosphere surrounding nucleic acids is extremely complex and dynamic, and difficult to study effectively [6]. Experimental studies of detailed Na^+ binding to the backbone, major, or minor groove are hindered by the difficulty of observing Na^+ experimentally by X-ray crystallography [7]. Molecular mechanics theoretical studies have indicated the presence of cations not only along the backbone but also within the major and minor grooves of DNA [8–10]. Simulations have also indicated the presence of Na^+ near G·C base pairs [11]. The difficulty of probing these structures experimentally has led to the continued use of molecular mechanics simulations to complement and further understand experimental results. Probing the noncovalent binding of alkali metal cations to nucleic acid monomers in the absence of solvent and the polymer scaffold offers the opportunity to understand intrinsic binding preferences and conformational changes and contribute to the computational models used to study these interactions in DNA and RNA. Similar studies have probed the binding of transition metal cations, such as Pb^{2+}, Zn^{2+}, and Pt^{2+}, to nucleic acid monomers, to explore the impact these metal ions have on conformation [12–17].

Infrared ion spectroscopy (IRIS), and specifically, infrared multiple photon dissociation (IRMPD) action spectroscopy, is proving to be an effective tool for probing the intrinsic gas phase structure of covalently and noncovalently bound systems [18–20]. In conjunction with theoretical calculations, the much narrower IR peak widths of IRMPD, in the absence of solvent and intermolecular interactions, allow for detailed study of the conformations accessed in the experiments [21–26]. Detailed electronic structure calculations allow for the analysis of experimental IRMPD action spectra, elucidation of the specific conformations and binding motifs accessed experimentally, and also provide insight into the potential energy surface of the ions of interest [24, 27].

The gas-phase structures and cationization of cytosine-based nucleic acid building blocks has been extensively studied by IRMPD [23, 24, 28–38]. Understanding the intrinsic behavior of these small nucleic acid monomers and their components in the gas phase allows for detailed study of the impact of specific components of the monomer, different ionization methods, and modification of their structures and properties. The IRMPD action spectra of the sodium-cationized forms of the DNA and RNA cytidine mononucleotides, 2′-deoxycytidine-5′-monophosphate (pdCyd) and cytidine-5′-monophosphate (pCyd), along with complimentary theoretical calculations, are detailed in this work. This data offers the opportunity to examine the impact of the sodium cation on intrinsic mononucleotide structure, and the impact of the phosphate moiety on sodium cation binding preferences. The structure and atom numbering of the cytidine mononucleotides are shown in Figure 1 with the nucleobase, nucleoside, and phosphate components labeled.

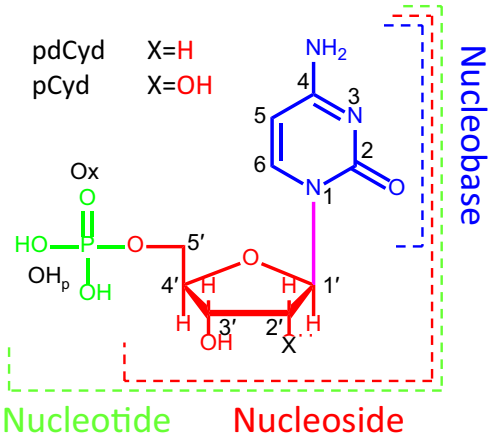

Figure 1. The chemical structure of the cytidine mononucleotides, 2′-deoxycytidine-5′-monophosphate (pdCyd), and cytidine-5′-monophosphate (pCyd), broken down into its component nucleobase, nucleoside, and phosphate moiety. The atom numbering of the nucleobase, sugar moiety, and phosphate moiety is also shown

Experimental Method

IRMPD Action Spectroscopy

IRMPD action spectroscopy experiments of $[pCyd+Na]^+$ and $[pCyd+Na]^+$ in the IR fingerprint region between 600 and 1800 cm^{-1} were performed using a custom-built 4.7-T Fourier-transform ion cyclotron resonance mass spectrometer (FT-ICR MS) coupled to the FELIX free electron laser (FEL, 10 Hz repetition rate, bandwidth 0.3% of the central frequency, energy up to 70 mJ/pulse) [39]. Ions were generated by electrospray ionization (ESI) from solutions of ~1 mM of pCyd or pdCyd in a 50%/50% methanol/water mixture with ~1 mM of NaCl added to promote sodium cationization. pCyd was purchased from TCI Europe, Zwijndrecht, Belgium, whereas pdCyd, NaCl, and solvents were purchased from Sigma-Aldrich, Zwijndrecht, The Netherlands. A detailed description of the instrument can be found elsewhere [39]. Following the electrospray ionization (ESI) source, the ions are accumulated in a hexapole ion guide before they are injected into the ICR cell through a DC quadrupole bender and octopole ion guide. The ions of interest are isolated in the ICR cell using stored waveform inverse Fourier transform (SWIFT) techniques and then irradiated for 3–4 s by the FEL. Any resultant product ions and remaining precursor ions are detected in the ICR cell. An IRMPD action spectrum is acquired by scanning the FEL across the region of interest, collecting ion intensities as a function of vibrational frequency. Precursor ion intensities (I_p) and fragment ion intensities (I_{f_i}) are then converted to an IRMPD yield using Eq. (1) below and plotted as a function of vibrational frequency.

$$\text{IRMPD yield} = \sum_i I_{f_i} / \left(I_p + \sum_i I_{f_i}\right) \quad (1)$$

The IRMPD action spectra in the hydrogen-stretching region were measured in much the same way using a modified Bruker amaZon ETD 3D quadrupole ion trap mass spectrometer (QIT MS) described in detail elsewhere [40, 41]. Ions were once again produced by ESI from solutions of ~25 μM of either pdCyd or pCyd and NaCl in 50%:50% methanol/water. The cytidine mononucleotides, pdCyd and pCyd, were purchased from Chem-Impex, Wood Dale, IL, USA, the HPLC-grade methanol and water were purchased from Sigma-Aldrich, St. Louis, MO, USA, and acetic acid was purchased from Fischer Scientific, Waltham, MA, USA. Following the ESI source, the ions are injected into the quadrupole ion trap through a transfer capillary, dual ion funnel, and octopole ion guide interface. The ions of interest were mass isolated and irradiated for 0.5 s by an optical parametric oscillator/amplifier (OPO) laser (Laservision, Bellevue, WA, USA, repetition rate 10 Hz, bandwidth 3 cm^{-1}, energy up to 15 mJ/pulse). Resultant fragment ions and remaining precursor ions were then detected and converted to an IRMPD yield that was plotted against vibrational frequency to produce the measured IRMPD action spectrum.

Theoretical Methods

Detailed analysis of IRMPD action spectra generally relies upon detailed electronic structure calculations to predict vibrational frequencies and visually analyze the agreement between the predicted frequencies and the measured IRMPD spectrum. To effectively perform this analysis, a variety of diverse conformations must be analyzed. A molecular mechanics conformational search is utilized to generate a range of conformations and Na^+-binding modes. The initial structures for the conformational search of the sodium-cationized cytidine mononucleotides included structures in which Na^+ was bound solely to O2, N3, O4′, O2′, Ox, or OH_p atoms, where Ox and OH_p are oxo and hydroxy oxygen atoms of the phosphate moiety. The neutral forms of pCyd and pdCyd were also subjected to the conformational search. Each initial structure was subjected to a simulated annealing procedure in HyperChem 8.0 [42] using the Amber 3 force field involving 3000 cycles of annealing. Each cycle consisted of 0.3 ps of heating from 0 to 1000 K, 0.2 ps to sample conformational space at 1000 K, and 0.3 ps of cooling from 1000 to 0 K. The resultant candidate structures were then submitted to a comparative structural analysis described in detail elsewhere [27] to evaluate the root mean squared deviation (RMSD) among them in order to determine which of the candidate structures found in the annealing procedures are structurally unique and low in energy. These unique conformations were submitted to a preliminary quantum mechanics structural optimization using the Gaussian 09 suite [43] and density functional theory (DFT) at the B3LYP/6-31+G(d) level of theory to better refine the structure. The RMSD structural analysis was used on the resultant structures to enable elimination of those candidate structures whose conformations had collapsed upon one another; the resultant "unique" conformers were then subjected to geometry optimization and frequency analyses at the B3LYP/6-311+G(d,p) level of theory. This level of theory has been shown to produce stable conformers and predict vibrational frequencies for the IRMPD analysis reasonably well for similar systems [31, 32, 35]. These conformers were also subjected to a further single-point energy calculation at the B3LYP/6-311+G(2d,2p) level of theory to better predict their relative Gibbs energies. The MP2 level of theory has also been used in several previous studies to calculate single-point energies of similar species with good results [33–35, 44]. However, in our past work [32–35, 45–56], B3LYP was found to perform at least as well as MP2 and often much better at describing the nucleic acid building blocks.

The specific conformations of the nucleotides are described using standard labels for nucleobase orientation and sugar puckering, as described in detail elsewhere [57]. The puckering of the sugar is described through calculation of a pseudorotation angle from the five dihedral angles of the sugar ring, and assigned a specific puckering mode, which is further simplified using the more traditional C2′-*endo*/C2′-*exo* nomenclature, indicating that the atom that deviates most from the plane of the sugar, C2′ in this example, lies either above (*endo*), on the same side as the nucleobase, or below (*exo*) the plane defined by the other three atoms of the sugar ring. The orientation of the cytosine nucleobase is described as *anti*, when it is oriented in such a way as to facilitate Watson–Crick base pairing, with the N3 and O2 atoms pointed away from the sugar moiety, or *syn* where the N3 and O2 atoms are oriented above/towards the sugar moiety. This orientation is calculated from the glycosidic bond dihedral angle, ∠O4′C1′N1C2. The orientation of the phosphate moiety can be described by the dihedral angle of the 5′-substituent, ∠O4′C4′C5′O5′, and the phosphate dihedral angle, ∠C4′C5′O5′P. The rotation of the phosphate moiety itself around the O5′–P bond appears to be less indicative of the orientation of the phosphate moiety within the conformer and was not incorporated. The location of the sodium cation is generally described relative to the sugar ring from the perspective of the C2′–C3′ side of the ring with the nucleobase and phosphate moiety located "above" the sugar ring. Individual conformers are assigned numerical designations based on their relative energetics within the bidentate (B), tridentate (T), or tetradentate (Q) sodium cation binding modes, with T1 being the most stable tridentate conformer, B1 the most stable bidentate conformer, and Q1 the most stable tetradentate conformer, regardless of the specific binding mode.

The predicted vibrational frequencies were calculated using the harmonic approximation, whereas the measured IRMPD spectrum is subject to the anharmonicity present in the real system. To approximately correct for the lack of anharmonicity in the predicted vibrational frequencies, scaling factors were used. Approximate scale factors were initially chosen based on literature precedence, and then slightly refined by visual comparison of all of the predicted IR spectra and the measured IRMPD spectrum, to achieve the best agreement between the dominant features. Once approximate values for the scaling factors have been determined in this way, more detailed comparisons between the measured IRMPD spectrum and the IR

spectra predicted for the ground and low-energy conformers computed as well as any others that appear to provide reasonable agreement with the measured spectrum are performed to further refine the scale factor applied. Historically, it has been well established that the anharmonicity of vibrational modes in the IR fingerprint and hydrogen-stretching regions were sufficiently different so as to require separate scaling factors. Thus, a distinct scale factor for each region has typically been applied to the predicted IR spectra before comparison to the experimental data. However, previous investigations have found that a single-scale factor does not enable the predicted IR spectra to accurately describe the measured IRMPD spectra of mononucleotides over the IR fingerprint region, a difficulty largely associated with the anharmonicity of the spectral features of the phosphate moiety [16, 17, 35, 38, 50–52, 58–60]. Although not a perfect solution, improved reproduction of the measured spectra was achieved by applying different scale factors to the vibrational frequencies above and below 1300 cm^{-1} in the IR fingerprint region. Consistent with these earlier works, the application of dual scaling factors over the IR fingerprint region also proved necessary for $[pdCyd+Na]^+$ and $[pCyd+Na]^+$, with vibrational frequencies below 1300 cm^{-1} scaled by 0.990 and those above 1300 cm^{-1} scaled by 0.978. As already well accepted, a different scale factor, 0.9615, is used for the hydrogen-stretching vibrations. To facilitate the analysis, the calculated and scaled vibrational frequencies are then convoluted with a Gaussian peak shape with a 20 cm^{-1} full width at half maximum (fwhm) in the IR fingerprint region to best capture the experimental peak widths, and a 15 cm^{-1} fwhm Gaussian peak shape in the hydrogen-stretching region.

Results

IRMPD Action Spectroscopy

The primary photofragment of both $[pCyd+Na]^+$ and $[pdCyd+Na]^+$ is $[Cyt+Na]^+$, the sodium-cationized cytosine nucleobase. This was the only fragment reliably observed in the experiments in the hydrogen-stretching region. However, minor photofragments were observed in the IR fingerprint region experiments, namely, the ion resulting from loss of H_2O from the precursor ion, and sodium-cationized phosphoric acid, $[H_3PO_4+Na]^+$. The experimental IRMPD action spectra of $[pdCyd+Na]^+$ and $[pCyd+Na]^+$ reported in this work are compared with those measured in previous work for the sodium cationized cytidine nucleosides, $[dCyd+Na]^+$ and $[Cyd+Na]^+$, as well as those of the protonated cytidine monophosphate nucleotides, $[pdCyd+H]^+$ and $[pCyd+H]^+$, in Figure 2. Immediately evident in Figure 2 are the significant parallels of the measured IRMPD spectra of the sodium-cationized cytidine nucleotides with the sodium-cationized nucleosides, particularly in the IR fingerprint region above 1300 cm^{-1}, where the measured features at ~1368, 1480, 1524, 1600, and 1650 cm^{-1} are all extremely parallel in shape and center to those measured for the sodium-cationized cytidine nucleosides. Below 1300 cm^{-1}, the measured spectra of

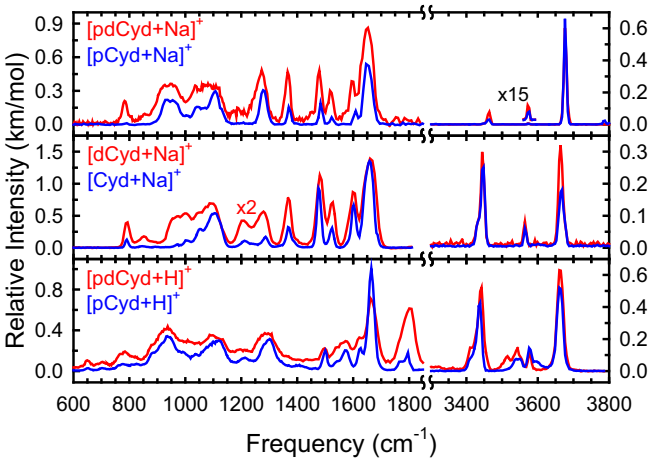

Figure 2. Comparison of experimental IRMPD action spectra of the sodium-cationized cytidine mononucleotides, $[pdCyd+Na]^+$ and $[pCyd+Na]^+$, the sodium-cationized cytidine nucleosides, $[dCyd+Na]^+$ and $[Cyd+Na]^+$, and the protonated cytidine mononucleotides $[pdCyd+H]^+$ and $[pCyd+H]^+$. Data for the sodium cationized cytidine nucleosides and protonated cytidine mononucleotides are taken from references [26, 29], respectively

$[pdCyd+Na]^+$ and $[pCyd+Na]^+$, with two complex features centered at ~982 and 1075 cm^{-1}, are more parallel in shape and position to that observed for $[dCyd+Na]^+$ than $[Cyd+Na]^+$. The measured IRMPD action spectra in the IR fingerprint region are also quite parallel, although the features measured in this work at ~3460 and 3568 cm^{-1} are much less intense than the analogous features measured for the sodium-cationized cytidine nucleosides, which is likely a result of differences in the ion cloud-laser light overlap due to their acquisition on the QIT MS instrument [40]. In comparison with the IRMPD action spectra of the protonated cytidine nucleotide analogues, several notable differences are evident. Perhaps the most important difference is the feature measured for $[pdCyd+H]^+$ and $[pCyd+H]^+$ at ~1808 cm^{-1}, corresponding to the free C2=O2 carbonyl stretch. This feature is not observed for either sodium-cationized cytidine mononucleotide or the sodium-cationized cytidine nucleosides, an indication that the noncovalently bound sodium cation is interacting with the O2-carbonyl oxygen atom.

Theoretical Results

The calculated ground conformers of the cytidine mononucleotides, pdCyd and pCyd, as well as those of their sodium-cationized forms, $[pdCyd+Na]^+$ and $[pCyd+Na]^+$, are shown in Figure 3. The computed ground conformers of $[pdCyd+Na]^+$ and $[pCyd+Na]^+$ both display tridentate noncovalent binding of the sodium cation to the oxo oxygen atom of the phosphate moiety (Ox), and the N3 and O2 atoms of the nucleobase, denoted as **T1(OxO2N3)**. Images of representative structures calculated for $[pdCyd+Na]^+$ and $[pCyd+Na]^+$ are shown in Figures S1 and S2, respectively, along with their conformer designation, nucleobase orientation, sugar puckering, and

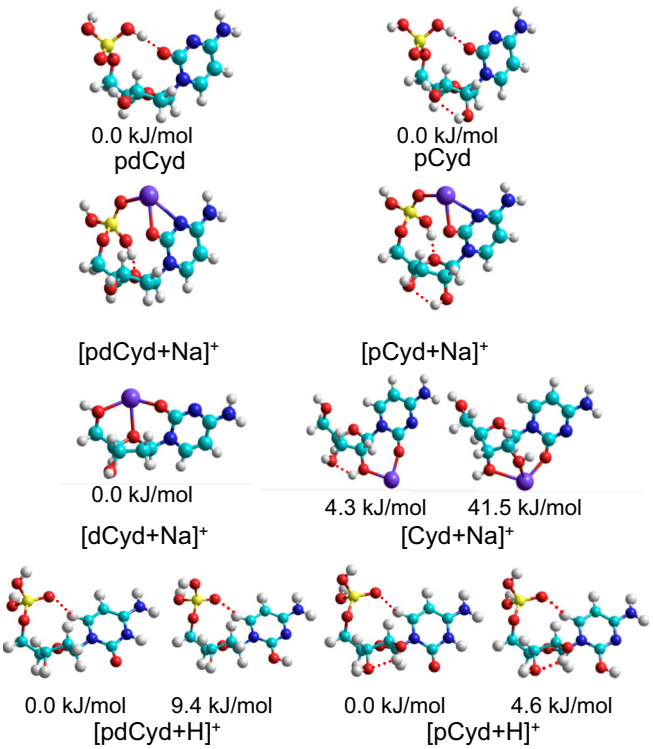

Figure 3. The calculated ground conformers of the neutral and sodium-cationized forms of the cytidine mononucleotides, pdCyd, pCyd, [pdCyd+Na]$^+$, and [pCyd+Na]$^+$, determined in the work. Also included are spectroscopically important conformers of the sodium-cationized forms of the cytidine nucleosides, [dCyd+Na]$^+$ and [Cyd+Na]$^+$, as well as the protonated cytidine mononucleotides, [pdCyd+H]$^+$ and and [pCyd+H]$^+$, determined in previous work [26,29]. All ground conformers were calculated at the B3LYP/6-311+G(2d,2p)//B3LYP/6-311+G(d,p) level of theory

relative Gibbs energies. Tables S1 and S2 list the relative Gibbs energies, calculated structural parameters, and labeled orientations of these representative structures for reference. The ground conformers, for both [pdCyd+Na]$^+$ and [pCyd+Na]$^+$, display a preference for the *syn* orientation of the nucleobase as well as C4′-*exo* sugar puckering, although a variety of sugar puckers are observed within 12 kJ/mol, all displaying the same T(OxO2N3) sodium cation–binding mode. The phosphate moiety also appears to be quite flexible within these low-lying tridentate conformers, with several different rotations of the ∠O4′C4′C5′O5′ and ∠C4′C5′O5′P dihedral angles observed within this 12 kJ/mol range. The ground conformers of both [pdCyd+Na]$^+$ and [pCyd+Na]$^+$ display an additional OH_p···O4′ intramolecular hydrogen-bonding interaction, and all of the low-energy conformers of [pCyd+Na]$^+$ also engage in a hydrogen-bonding interaction between the 2′- and 3′-hydroxy substituents.

The second most stable cation binding mode found is also tridentate, T(OxO4′O2). The most stable examples of this binding mode, **T9$_{pdCyd}$(OxO4′O2)** and **T8$_{pCyd}$(OxO4′O2)**, are found to be 9.0 and 14.9 kJ/mol higher in Gibbs energy than the calculated **T1(OxO2N3)** ground conformers of [pdCyd+Na]$^+$ and [pCyd+Na]$^+$, respectively. The sodium cation of **T9$_{pdCyd}$(OxO4′O2)** and **T8$_{pCyd}$(OxO4′O2)** is bound behind the plane of the sugar ring, looking from the C2′ and C3′ atoms. In these conformers, the sodium cation lies slightly above and behind the sugar ring, whereas in the **T10$_{pdCyd}$(OxO4′O2)** and **T10$_{pCyd}$(OxO4′O2)**, the next most stable T(OxO4′O2) conformers, the sodium cation is bound slightly below and behind the sugar ring. The most stable conformers exhibiting this T(OxO4′O2) binding mode both exhibit C3′-*endo* sugar puckering with *syn* nucleobase orientations, but conformers exhibiting C2′-*endo* puckering are found close in Gibbs energy, ≤2.8 kJ/mol. Another form of the T(OxO4′O2) binding mode is observed in **T13$_{pdCyd}$(OxO4′O2)** and **T11$_{pCyd}$(OxO4′O2)**, lying 16.2 and 21.9 kJ/mol above the respective T(OxO2N3) ground conformers. In these conformers, the sodium cation is bound more directly above the O4′ atom, and not behind the sugar moiety, similar to the calculated ground conformer of [dCyd+Na]$^+$, shown in Figure 3.

The most stable bidentate cation binding mode is B(OxO2), observed as **B1$_{dCyd}$(OxO2)** and **B1$_{pCyd}$(OxO2)**, lying 9.9 and 16.1 kJ/mol higher than the calculated ground conformers, respectively. The orientation of the phosphate moiety in the B(OxO2) conformers is notably different than that observed in the T(OxO2N3) conformers. The phosphate moiety in B(OxO2) conformers is oriented away from the sugar ring, rather than above or behind as observed in the low-energy tridentate conformers. Another bidentate binding mode, B(O2N3), is observed in **B3$_{pdCyd}$(O2N3)** and **B3$_{Cyd}$(O2N3)**, which lie 49.7 and 56.6 kJ/mol higher in relative Gibbs energy, respectively. Binding of the sodium cation solely to the nucleobase allows for a great deal of flexibility in both the nucleobase orientation and the phosphate moiety, and several such conformations were calculated, with only the most stable of these conformers shown in Figures S1 and S2, as they lie so high in relative Gibbs energy. For [pCyd+Na]$^+$, a unique bidentate binding mode, B(O2O2′), is observed in conformer **B2$_{pCyd}$(O2O2′)**, lying 29.3 kJ/mol above the **T1$_{Cyd}$** ground conformer. The B(O2O2′) binding mode restricts the nucleobase orientation but leaves the phosphate moiety free, so although many more conformers of this type were calculated, only the most stable conformer calculated, **B2$_{pCyd}$(O2O2′)**, is shown. Tetradentate binding modes were also observed. The **Q1(O4′O5′O2OH$_p$)** sodium cation binding mode is found 41.0 and 46.4 kJ/mol higher in energy than the respective ground conformers of [pdCyd+Na]$^+$ and [pCyd+Na]$^+$. Another tetradentate binding mode, Q(OxO4′O2OH$_p$), is found only for [pCyd+Na]$^+$, displaying a highly parallel structure but with a different phosphate orientation facilitating interaction with the oxo atom of the phosphate instead of the 5′-hydroxy oxygen atom. Although this binding mode was only observed in these calculations for [pCyd+Na]$^+$, the lack of interaction between the sodium cation and 2′-hydroxy substituent indicates that it is a potential binding mode for [pdCyd+Na]$^+$. These tetradentate binding modes are similar to several of the T(OxO4′O2) conformers in nucleobase orientation, with glycosidic bond angles

of ~300°, and the sodium cation bound "behind" the sugar ring. Overall, sugar puckering appears to be less important to conformer stability than previously observed for the nucleoside analogues, with relative stability driven primarily by the mode of binding and the orientation of the phosphate moiety. This reduced impact of sugar puckering might be due to the increased flexibility afforded to the phosphate moiety in the nucleotide over the 5′-hydroxy substituent in the nucleosides, allowing for the optimal cation binding mode to be found under different sugar puckering conditions.

Representative conformers of the neutral forms of pdCyd and pCyd are shown in Figures S3 and S4 along with their conformer designation, nucleobase orientation, sugar puckering, and relative Gibbs energies. Tables S3 and S4 list the relative Gibbs energies, calculated structural parameters, and labeled orientations of these representative structures for reference. Both pdCyd and pCyd favor conformers displaying simultaneous OH_p···O2 and O3′H···Ox intramolecular hydrogen-bonding interactions stabilizing the nucleobase and phosphate moieties. Stabilization of the nucleobase orientation appears to be favored over stabilization of the phosphate moiety. A conformer of pCyd lying only 4.3 kJ/mol above the ground conformer displays O3′H···O2′H···O2 hydrogen-bonding interactions, stabilizing the nucleobase orientation to the sugar ring, with no obvious hydrogen-bonding interactions stabilizing the phosphate moiety, whereas conformers of pdCyd and pCyd stabilizing the phosphate moiety and not the nucleobase orientation lie 15.7 and 16.6 kJ/mol above the ground conformers, respectively.

The spectroscopically important conformers of the sodium-cationized forms of the cytidine nucleosides, $[dCyd+Na]^+$ and $[Cyd+Na]^+$, as well as those of the protonated forms of the cytidine mononucleotides, $[pdCyd+H]^+$ and $[pCyd+H]^+$, determined in previous work, are also shown in Figure 3 for comparison [31, 35].

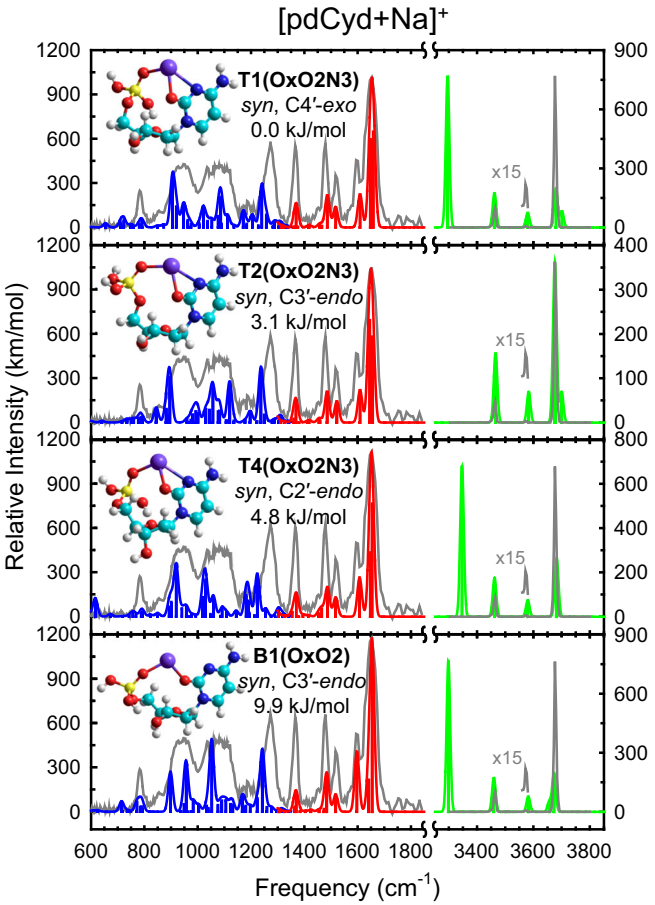

Figure 4. Comparison of the measured IRMPD action spectrum of $[pdCyd+Na]^+$ with the B3LYP/6-311+G(d,p) predicted linear IR spectra for representative low-energy conformers that are populated in the experiments. The sodium cation binding mode, nucleobase orientation, sugar puckering, and relative B3LYP/6-311+G(2d,2p) Gibbs energies at 298 K are indicated for each conformer. The measured IRMPD action spectrum is superimposed on the calculated spectra and the intensity scaled to facilitate comparisons

Discussion

Experimentally Populated Conformers of $[pdCyd+Na]^+$

The experimental IRMPD action spectrum and predicted IR spectra of interesting and representative low-energy conformers of $[pdCyd+Na]^+$ are compared in Figure 4. A more thorough set of representative conformers of $[pdCyd+Na]^+$ are shown in Figure S1, and their predicted IR spectra are compared with the experimental IRMPD spectrum in Figure S5. The difficulty in finding a single scaling factor to treat the region below 1300 cm^{-1} results in a compromise, notably observed in the feature at ~1273 cm^{-1}, which is not well represented by any of the predicted IR spectra shown in Figure 4 or Figure S5 and corresponds to the P–Ox/P=Ox stretch. Another notable issue in the analysis of the conformers populated in the experiments is the width of the features at ~982 and 1075 cm^{-1}, which is not represented well by any single conformer, and indicates that multiple conformers may be present. The smaller features measured at ~1368, 1480, and 1524 cm^{-1} are all reasonably well represented by the four conformers **$T1_{pdCyd}$(OxO2N3)**, **$T2_{pdCyd}$(OxO2N3)**, **$T4_{pdCyd}$(OxO2N3)**, and **$B1_{pdCyd}$(OxO2)** shown in Figure 4, as well as every conformer shown in Figure S5. However, the major feature at ~1650 cm^{-1}, arising from the symmetric NH_2 bending of the nucleobase, provides better differentiation between the predicted IR spectra shown in Figure S5. Conformers displaying the T(OxO4′O2) sodium binding mode, such as **$T9_{pdCyd}$(OxO4′O2)**, generally predict the shape of this feature poorly, with more separation between the intense NH_2 bending and less intense NH_2 bending coupled to C–H bending in the nucleobase vibrational modes. The T(OxO4′O2) conformers also predict the center of this feature to be slightly blue shifted relative to the measured band. This measured feature is also predicted somewhat poorly by the **$B3_{pdCyd}$(O2N3)** conformer, which predicts a slight red shift of this feature. In the hydrogen-stretching region, these T(OxO4′O2) and B(O2N3) conformers also predict the

measured feature at ~3676 cm^{-1} poorly, being somewhat red shifted and split for the T(OxO4′O2) conformers and slightly blue shifted for the B(O2N3) conformers. Even more blatant examples of spectral disagreement in the hydrogen-stretching region would appear to be the intense features around ~3300–3350 cm^{-1} in the spectra of **T4$_{pdCyd}$(OxO2N3)** and **B1$_{pdCyd}$(OxO2)** conformers. However, this predicted feature results from the OH_p stretch, which is involved in the OH_p···O4′ hydrogen-bonding interaction in those conformers, and as such may not be observed there experimentally as the anharmonicity of the hydrogen-bonding vibrational mode could shift its frequency and intensity [61–63].

Visual analysis of the measured IRMPD spectrum and the predicted IR spectra suggests that the conformers populated in the experiment have structures similar to the **T4$_{pdCyd}$(OxO2N3)** and **B1$_{pdCyd}$(OxO2)** conformers shown in Figure 4. These conformers are generally best described by a glycosidic bond angle of ~70°, with a remarkably flexible sugar pucker and phosphate orientation. Some conformers such as **T13$_{pdCyd}$(OxO4′O2)**, with the sodium bound above the sugar ring, on the same side as the nucleobase, display similar glycosidic bond angles but with predicted IR spectra more consistent with the other T(OxO4′O2) conformers, described above, but these conformers display greater disagreement with the measured spectrum. The measured spectrum between 1300 and 1800 cm^{-1} is well reproduced by the tridentate T(OxO2N3) and bidentate B(OxO2) conformers, **T1–T8**, **T11**, **B1**, and **B2** of $[pdCyd+Na]^+$, all of which display parallel structures. However, some differences in the spectra of several of these conformers such as **T1–T3** are seen in the hydrogen-stretching region, most notably the small shoulder attributed to the O3′–H stretch at ~3690 cm^{-1}. **T4$_{pdCyd}$(OxO2N3)** appears to provide the best overall agreement with the measured spectrum, but it is likely that a mixture of the **T1–T8**, **B1**, and **B2** conformers is present in the experiments, contributing to the broad width of the measured features at ~982 and 1075 cm^{-1}. Vibrational assignments based upon these conformers are given in Table S5.

Experimentally Populated Conformers of $[pCyd+Na]^+$

The experimental IRMPD action spectrum and predicted IR spectra of several representative low-energy conformers of $[pCyd+Na]^+$ are compared in Figure 5. Additional spectral comparisons with a broader selection of representative conformers are shown in Figure S6. Similar to $[pdCyd+Na]^+$, selection of a scaling factor to treat the vibrations below 1300 cm^{-1} in $[pCyd+Na]^+$ is challenging, due once again to the feature at ~1283 cm^{-1}. In every theoretical IR spectrum, this feature is predicted somewhat poorly in order to achieve better agreement with the features at ~955 and 1107 cm^{-1}. As in $[pdCyd+Na]^+$, the feature at ~1283 cm^{-1} corresponds to the P–Ox/P=Ox stretch, which is involved in binding of the sodium cation. The two complex features at ~955 and 1107 cm^{-1} present better peak shapes for visual matching to the predicted IR spectra of $[pCyd+Na]^+$ than that observed for $[pdCyd+Na]^+$,

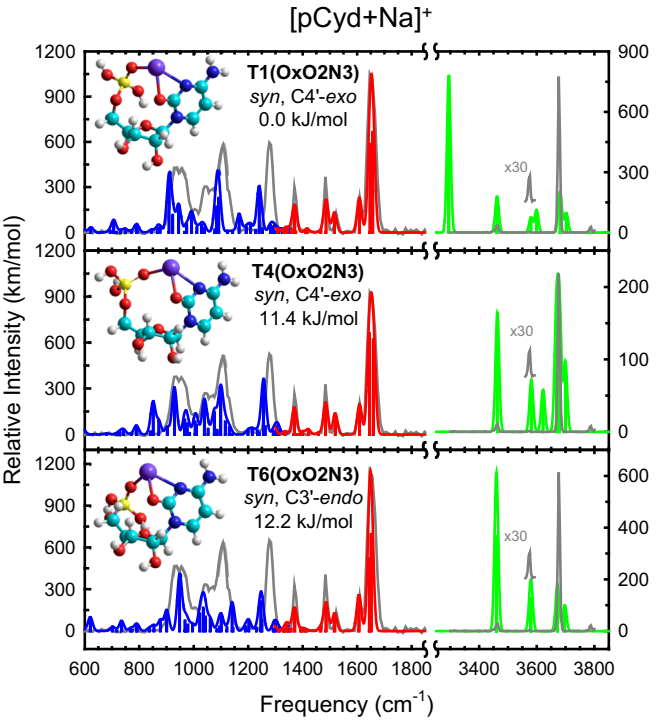

Figure 5. Comparison of the measured IRMPD action spectrum of $[pCyd+Na]^+$ with the B3LYP/6-311+G(d,p) predicted linear IR spectra for representative low-energy conformers that are populated in the experiments. The sodium cation binding mode, nucleobase orientation, sugar puckering, and relative B3LYP/6-311+G(2d,2p) Gibbs energies at 298 K are indicated for each conformer. The measured IRMPD action spectrum is superimposed on the calculated spectra and the intensity scaled to facilitate comparisons

and several T(OxO2N3) binding conformers provide reasonable agreement with these features. Between 1300 and 1700 cm^{-1}, all of the T(OxO2N3) binding conformers display good agreement with the measured spectrum. In contrast, conformers with alternate binding modes such as T(OxO4′O2), T(O5′O2OH_p), T(OxO4′O5′), Q(O4′O5′OH_pO2), and B(O2N3) disagree with the measured peak shape at ~1645 cm^{-1}, precluding conformations involving these modes of Na^+ binding from significant contribution to the experimental spectrum. Although **B1$_{pCyd}$(OxO2)** presents reasonable agreement with the measured spectrum across the IR fingerprint region, misalignment with the measured feature at ~1645 cm^{-1} indicates that it cannot be making a significant contribution to the measured spectrum. Among the low-energy T(OxO2N3) binding conformers that offer good agreement with the measured spectrum in the IR fingerprint region, **T1–T7**, relatively consistent disagreements are observed in the hydrogen-stretching region. Consistent among **T1–T7** is a predicted vibrational mode at ~3700 cm^{-1} that does not provide a match for any measured feature. This feature corresponds to the O3′–H stretch, and in each of these conformers, the 3′-hydroxy oxygen atom is acting as either a hydrogen-bond donor or acceptor and as such the intensity is predicted poorly by the harmonic calculations, or not captured well in the measured spectrum. Similarly, the

vibrational mode predicted to lie between the measured features at ~3572 and ~3675 cm^{-1}, which does not match any measured features, corresponds to the O2′–H stretch, which is also involved directly or indirectly in hydrogen-bonding interactions. **$T6_{pCyd}$(OxO2N3)** does not display this feature between ~3572 and ~3675 cm^{-1} as it has collapsed upon the asymmetric NH_2 stretch at ~3572 cm^{-1}. Similar to that observed for $[pdCyd+Na]^+$, conformers **$T1_{pCyd}$(OxO2N3)** and **$T3_{pCyd}$(OxO2N3)**, which display OH_p···O4′ hydrogen-bonding interactions also predict a corresponding feature between ~3300 and 3360 cm^{-1} that is not experimentally observed in this frequency range, as expected given its involvement in a hydrogen-bonding interaction.

Low-energy conformers with the tridentate binding mode T(OxO2N3) provide the best spectral representation of the experimental spectrum. Specifically, a mixture of the **$T1_{pCyd}$–$T7_{pCyd}$** conformers provides good representation when considering that the O2′–H and O3′–H stretches in the hydrogen-stretching region may have been too weak to measure in the experiment or have shifted due to the greater anharmonicity introduced via hydrogen-bonding interactions. These O2′–H and O3′–H stretches are predicted for all of the conformers calculated except those displaying B(O2O2′) binding; the predicted spectrum of these latter conformers provides poorer agreement in the hydrogen-stretching region. **$T4_{pCyd}$(OxO2N3)** provides the best overall match to the experimental spectrum in the IR fingerprint region and decent agreement in the hydrogen-stretching region, comparable to the other low-energy T(OxO2N3) conformers. Vibrational assignments based upon these conformers are given in Table S6.

Comparison to Sodium-Cationized Cytidine Nucleosides

The calculated ground conformers of both sodium-cationized DNA and RNA cytidine nucleosides $[dCyd+Na]^+$ and $[Cyd+Na]^+$ exhibit tridentate T(O5′O4′O2) binding [31]. However, this binding mode is not favored experimentally for $[Cyd+Na]^+$ where B(O2O2′) and T(O2O2′O3′) binding modes are observed, kinetically trapped from solvated structures. The bidentate **$B2_{pCyd}$(O2O2′)** binding mode of $[pCyd+Na]^+$ parallels the **B1(O2O2′)** conformer of $[Cyd+Na]^+$, but lies much higher in relative Gibbs energy to the calculated ground conformer and displays spectral disagreement that precludes it from significant contribution to the experimental spectrum. For $[dCyd+Na]^+$, the predicted T(O5′O4′O2) binding mode, as observed in the calculated ground conformer, is spectroscopically preferred. The most parallel binding mode to this $[dCyd+Na]^+$ ground conformer in the cytidine mononucleotides is the T(OxO4′O2) binding mode, specifically the higher energy version of this binding mode where the sodium cation lies almost directly above the O4′ atom, which lies 16.2 and 21.9 kJ/mol higher in Gibbs energy for $[pdCyd+Na]^+$ and $[pCyd+Na]^+$, respectively. Consistent between the nucleoside and mononucleotide is the preference for interaction of the sodium cation with both the sugar and nucleobase, providing stability to the glycosidic bond, as well as an energetic preference in the gas phase for simultaneous stabilization of the nucleobase and the 5′-oxygen atom either directly or via the phosphate moiety.

Comparison to Protonated Cytidine Mononucleotides

The protonated cytidine mononucleotides, $[pdCyd+H]^+$ and $[pCyd+H]^+$, both prefer *anti* nucleobase orientations stabilized by C6H···Ox intramolecular hydrogen-bonding interactions [35]. As also observed in studies of the protonated cytidine nucleosides, conformers protonated at the N3 position and those protonated at the O2 position are experimentally populated. Unlike the sodium-cationized cytidine mononucleotides, and nucleosides as well, the protonated conformers display energetic and spectroscopic preference for "isolation" of the cation, preferring the proton not to have direct involvement in the hydrogen-bonding stabilization of the conformer. However, stabilization of the phosphate moiety and nucleobase orientation together is preferred regardless of the cationizing agent. Although conformations of $[pdCyd+H]^+$ and $[pCyd+H]^+$ exhibiting additional hydrogen-bonding interactions between the phosphate moiety and the sugar ring through O4′ are found, similar to the computed ground conformers of the sodium-cationized mononucleotides, these conformations were calculated to be slightly higher in Gibbs energy, and more importantly, not spectroscopically relevant.

Impact of Sodium Cationization on Cytidine Mononucleotide Structure

Neutral pdCyd and pCyd were both calculated to prefer conformers stabilizing both the phosphate moiety and nucleobase through an OH_p···O2 intramolecular hydrogen-bonding interaction, with the phosphate moiety also being stabilized to the sugar ring through an O3′H···Ox hydrogen-bonding interaction. This is reminiscent of the phosphate-nucleobase stabilization preferred by both $[pdCyd+Na]^+$ and $[pCyd+Na]^+$ in the form of the T(OxO2N3) binding mode. The calculated ground conformers of both nucleotides also display additional stabilization of the phosphate moiety to the sugar ring through an OH_p···O4′ hydrogen-bonding interaction. Conformers of the neutral cytidine nucleotides without phosphate-nucleobase stabilization can be found reasonably low in Gibbs energy, ~15.7 and 4.3 kJ/mol for pdCyd and pCyd. In contrast, conformers of $[pdCyd+Na]^+$ and $[pCyd+Na]^+$ without stabilization of the phosphate moiety to the nucleobase lie much higher in Gibbs energy, 49.7 and 29.3 kJ/mol for the **$B3_{pdCyd}$(O2N3)** and **$B2_{pCyd}$(O2O2′)** conformers, respectively.

Conclusions

IRMPD action spectroscopy of the sodium-cationized DNA and RNA cytidine mononucleotides reveals an energetic and spectroscopic preference for stabilization of the nucleobase and

phosphate moiety through a tridentate T(OxO2N3) cation binding mode. Although the method of stabilization is different, this is in good agreement with the calculations performed here for the neutral cytidine mononucleotides and previous observations regarding the protonated DNA and RNA cytidine mononucleotides. In each of these cases, the flexible phosphate moiety prefers to adopt an orientation that allows for either sodium cation binding, or a hydrogen-bonding interaction between phosphate and nucleobase, creating large and flexible chelation or hydrogen-bonding rings. In the sodium-cationized cytidine mononucleotides examined here, the most stable conformer observed, **T1(OxO2N3)**, also displays an additional $OH_p \cdots O4'$ hydrogen-bonding interaction, further stabilizing the orientation of the phosphate moiety to the sugar ring itself. The increased flexibility of the phosphate moiety of the mononucleotide over the 5′-hydroxy substituent of the nucleoside allows for more structural variety within low-lying conformers. The phosphate moiety also largely masks the influence of the sugar puckering on the predicted IR spectra, making differentiation between sugar puckering modes spectroscopically infeasible for the mononucleotides. Sodium cation binding via chelation to the nucleobase and phosphate moiety is heavily preferred over binding to the phosphate moiety or nucleobase independently.

Acknowledgements

Financial support for this work was provided by the National Science Foundation, grant numbers OISE-0730072 (for the FEL IRMPD measurements and international travel), DBI-0922818 (for the Bruker amaZon ETD QITMS), and CHE-1709789 (other research costs). Financial support of the FELIX facility by the Nederlandse Organisatie voor Wetenschappelijk Onderzoek (NWO) is also gratefully acknowledged. Support from the Thomas C. Rumble Graduate Fellowship is acknowledged by Y.-w. Nei and L.A. Hamlow, with additional support from a Wilfried Heller Research Fellowship and Wayne State University Summer Dissertation Fellowship by Y.-w. Nei. Computational resources for this work were provided by Wayne State University C&IT. The skilled assistance of the FELIX staff is also greatly appreciated.

References

1. Hanzlik, R.P., Inorganic aspects of biological and organic chemistry. Academic. Cambridge (1976)
2. Alberts, B., Dennis, B., Johnson, A., Lewis, J., Raff, M., Robert, K., Walter, P., Roberts, K.: Essential cell biology: an introduction to the molecular biology of the cell. Garland Publishing Inc., New York (1998)
3. Shinoda, T., Ogawa, H., Cornelius, F., Toyoshima, C.: Crystal structure of the sodium–potassium pump at 2.4 Å resolution. Nature. **459**, 446–450 (2009)
4. Morth, J.P., Pedersen, B.P., Toustrup-Jensen, M.S., Sørensen, T.L.M., Petersen, J., Andersen, J.P., Vilsen, B., Nissen, P.: Crystal structure of the sodium–potassium pump. Nature. **450**, 1043–1049 (2007)
5. Anastassopoulou, J.: Metal-DNA interactions. J. Mol. Struct. **651**, 19–26 (2003)
6. Lipfert, J., Doniach, S., Das, R., Herschlag, D.: Understanding nucleic acid-ion interactions. Annu. Rev. Biochem. **83**, 813–841 (2014)
7. Tereshko, V., Wilds, C.J., Minasov, G., Prakash, T.P., Maier, M.A., Howard, A., Wawrzak, Z., Manoharan, M., Egli, M.: Detection of alkali metal ions in DNA crystals using state-of-the-art X-ray diffraction experiments. Nucleic Acids Res. **29**, 1208–1215 (2001)
8. Korolev, N., Lyubartsev, A.P., Laaksonen, A., Nordenskiöld, L.: On the competition between water, sodium ions, and spermine in binding to DNA: a molecular dynamics computer simulation study. Biophys. J. **82**, 2860–2875 (2002)
9. Hud, N.V., Polak, M.: DNA–cation interactions: the major and minor grooves are flexible ionophores. Curr. Opin. Struc. Biol. **11**, 293–301 (2001)
10. Howerton, S.B., Sines, C.C., VanDerveer, D., Williams, L.D.: Locating monovalent cations in the grooves of B-DNA. Biochemistry. **40**, 10023–10031 (2001)
11. McConnell, K.J., Beveridge, D.L.: DNA structure: what's in charge? J. Mol. Biol. **304**, 803–820 (2000)
12. Salpin, J.-Y., Guillaumont, S., Ortiz, D., Tortajada, J., Maître, P.: Direct evidence for tautomerization of the uracil moiety within the Pb^{2+}/uridine-5′-monophosphate complex: a combined tandem mass spectrometry and IRMPD study. Inorg. Chem. **50**, 7769–7778 (2011)
13. Ciavardini, A., Dalla Cort, A., Fornarini, S., Scuderi, D., Giardini, A., Forte, G., Bodo, E., Piccirillo, S.: Adenosine monophosphate recognition by zinc–salophen complexes: IRMPD spectroscopy and quantum modeling study. J. Mol. Spectrosc. **335**, 108–116 (2017)
14. Salpin, J.-Y., Gamiette, L., Tortajada, J., Besson, T., Maître, P.: Structure of Pb^{2+}/dCMP and Pb^{2+}/CMP complexes as characterized by tandem mass spectrometry and IRMPD spectroscopy. Int. J. Mass Spectrom. **304**, 154–164 (2011)
15. Chiavarino, B., Crestoni, M.E., Fornarini, S., Scuderi, D., Salpin, J.-Y.: Undervalued N3 coordination revealed in the cisplatin complex with 2′-deoxyadenosine-5′-monophosphate by a combined IRMPD and theoretical study. Inorg. Chem. **56**, 8793–8801 (2017)
16. Chiavarino, B., Crestoni, M.E., Fornarini, S., Scuderi, D., Salpin, J.-Y.: Interaction of cisplatin with 5′-dGMP: a combined IRMPD and theoretical study. Inorg. Chem. **54**, 3513–3522 (2015)
17. Salpin, J.-Y., MacAleese, L., Chirot, F., Dugourd, P.: Structure of the Pb^{2+}–deprotonated dGMP complex in the gas phase: a combined MS-MS/IRMPD spectroscopy/ion mobility study. Phys. Chem. Chem. Phys. **16**, 14127–14138 (2014)
18. Fridgen, T.D.: Infrared consequence spectroscopy of gaseous protonated and metal ion cationized complexes. Mass Spectrom. Rev. **28**, 586–607 (2009)
19. MacAleese, L., Maitre, P.: Infrared spectroscopy of organometallic ions in the gas phase: from model to real world complexes. Mass Spectrom. Rev. **26**, 583–605 (2007)
20. Stedwell, C.N., Galindo, J.F., Roitberg, A.E., Polfer, N.C.: Structures of biomolecular ions in the gas phase probed by infrared light sources. Annu. Rev. Anal. Chem. **6**, 267–285 (2013)
21. Bush, M.F., O'Brien, J.T., Prell, J.S., Saykally, R.J., Williams, E.R.: Infrared spectroscopy of cationized arginine in the gas phase: direct evidence for the transition from nonzwitterionic to zwitterionic structure. J. Am. Chem. Soc. **129**, 1612–1622 (2007)
22. Abi-Ghanem, J., Gabelica, V.: Nucleic acid ion structures in the gas phase. Phys. Chem. Chem. Phys. **16**, 21204–21218 (2014)
23. Salpin, J.-Y., Guillaumont, S., Tortajada, J., MacAleese, L., Lemaire, J., Maitre, P.: Infrared spectra of protonated uracil, thymine and cytosine. ChemPhysChem. **8**, 2235–2244 (2007)
24. Filippi, A., Fraschetti, C., Rondino, F., Piccirillo, S., Steinmetz, V., Guidoni, L., Speranza, M.: Protonated pyrimidine nucleosides probed by IRMPD spectroscopy. Int. J. Mass Spectrom. **354-355**, 54–61 (2013)
25. Rajabi, K., Gillis, E.A.L., Fridgen, T.D.: Structures of alkali metal ion −adenine complexes and hydrated complexes by IRMPD spectroscopy and electronic structure calculations. J. Phys. Chem. A. **114**, 3449–3456 (2010)
26. Jašíková, L., Roithová, J.: Infrared multiphoton dissociation spectroscopy with free-electron lasers: on the road from small molecules to biomolecules. Chem.-Eur. J. **24**, 3374–3390 (2018)
27. Hamlow, L.A., Devereaux, Z.J., Roy, H.A., Cunningham, N.A., Berden, G., Oomens, J., Rodgers, M.T.: Impact of the 2′- and 3′-sugar hydroxyl moieties on gas-phase nucleoside structure. J. Am. Soc. Mass Spectrom. **30**, 832–845 (2019)

28. Yang, B., Wu, R.R., Berden, G., Oomens, J., Rodgers, M.T.: Infrared multiple photon dissociation action spectroscopy of proton-bound dimers of cytosine and modified cytosines: effects of modifications on gas-phase conformations. J. Phys. Chem. B. **117**, 14191–14201 (2013)
29. Yang, Z., Rodgers, M.T.: Theoretical studies of the unimolecular and bimolecular tautomerization of cytosine. Phys. Chem. Chem. Phys. **6**, 2749–2757 (2004)
30. Yang, Z., Rodgers, M.T.: Tautomerization in the formation and collision-induced dissociation of alkali metal cation-cytosine complexes. Phys. Chem. Chem. Phys. **14**, 4517–4526 (2012)
31. Zhu, Y., Hamlow, L.A., He, C.C., Roy, H.A., Cunningham, N.A., Munshi, M., Berden, G., Oomens, J., Rodgers, M.T.: Conformations and N-glycosidic bond stabilities of sodium cationized 2-deoxycytidine and cytidine: solution conformation of $[Cyd+Na]^+$ is preserved upon ESI. Int. J. Mass Spectrom. **429**, 18–27 (2018)
32. Wu, R., Yang, B., Frieler, C., Berden, G., Oomens, J., Rodgers, M.: N3 and O2 protonated tautomeric conformations of 2′-deoxycytidine and cytidine coexist in the gas phase. J. Phys. Chem. B. **119**, 5773–5784 (2015)
33. Nei, Y.W., Crampton, K.T., Berden, G., Oomens, J., Rodgers, M.T.: Infrared multiple photon dissociation action spectroscopy of deprotonated RNA mononucleotides: gas-phase conformations and energetics. J. Phys. Chem. A. **117**, 10634–10649 (2013)
34. Nei, Y.W., Hallowita, N., Steill, J.D., Oomens, J., Rodgers, M.T.: Infrared multiple photon dissociation action spectroscopy of deprotonated DNA mononucleotides: gas-phase conformations and energetics. J. Phys. Chem. A. **117**, 1319–1335 (2013)
35. Wu, R.R., Hamlow, L.A., He, C.C., Nei, Y.W., Berden, G., Oomens, J., Rodgers, M.T.: N3 and O2 protonated conformers of the cytosine mononucleotides coexist in the gas phase. J. Am. Soc. Mass Spectrom. **28**, 1638–1646 (2017)
36. Oomens, J., Moehlig, A.R., Morton, T.H.: Infrared multiple photon dissociation (IRMPD) spectroscopy of the proton-bound dimer of 1-methylcytosine in the gas phase. J. Phys. Chem. Lett. **1**, 2891–2897 (2010)
37. Gao, J., Berden, G., Rodgers, M.T., Oomens, J.: Interaction of Cu^+ with cytosine and formation of i-motif-like C–M^+–C complexes: alkali versus coinage metals. Phys. Chem. Chem. Phys. **18**, 7269–7277 (2016)
38. van Outersterp, R.E., Martens, J., Berden, G., Steill, J.D., Oomens, J., Rijs, A.M.: Structural characterization of nucleotide 5′-triphosphates by infrared ion spectroscopy and theoretical studies. Phys. Chem. Chem. Phys. **20**, 28319–28330 (2018)
39. Oomens, J.S., Sartakov, B., Meijer, G., von Helden, G.: Gas-phase infrared multiple photon dissociation spectroscopy of mass-selected molecular ions. Int. J. Mass Spectrom. **254**, 1–19 (2006)
40. Hamlow, L.A., Zhu, Y., Devereaux, Z.J., Cunningham, N.A., Berden, G., Oomens, J., Rodgers, M.T.: Modified quadrupole ion trap mass spectrometer for infrared ion spectroscopy: application to protonated thiated uridines. J. Am. Soc. Mass Spectrom. **29**, 2125–2137 (2018)
41. Martens, J., Berden, G., Gebhardt, C.R., Oomens, J.: Infrared ion spectroscopy in a modified quadrupole ion trap mass spectrometer at the FELIX free electron laser laboratory. Rev. Sci. Instrum. **87**, 103108–103108 (2016)
42. Kumar, R.K., Davis, D.R.: Synthesis and studies on the effect of 2-thiouridine and 4-thiouridine on sugar conformation and RNA duplex stability. Nucleic Acids Res. **25**, 1272–1280 (1997)
43. Frisch, M.J., Trucks, G.W., Schlegel, H.B., Scuseria, G.E., Robb, M.A., Cheeseman, J.R., Scalmani, G., Barone, V., Mennucci, B., Petersson, G.A., Nakatsuji, H., Caricato, M., Li, X., Hratchian, H.P., Izmaylov, A.F., Bloino, J., Zheng, G., Sonnenberg, J.L., Hada, M., Ehara, M., Toyota, K., Fukuda, R., Hasegawa, J., Ishida, M., Nakajima, T., Honda, Y., Kitao, O., Nakai, H., Vreven, T., Montgomery Jr., J.A., Peralta, J.E., Ogliaro, F., Bearpark, M.J., Heyd, J., Brothers, E.N., Kudin, K.N., Staroverov, V.N., Kobayashi, R., Normand, J., Raghavachari, K., Rendell, A.P., Burant, J.C., Iyengar, S.S., Tomasi, J., Cossi, M., Rega, N., Millam, N.J., Klene, M., Knox, J.E., Cross, J.B., Bakken, V., Adamo, C., Jaramillo, J., Gomperts, R., Stratmann, R.E., Yazyev, O., Austin, A.J., Cammi, R., Pomelli, C., Ochterski, J.W., Martin, R.L., Morokuma, K., Zakrzewski, V.G., Voth, G.A., Salvador, P., Dannenberg, J.J., Dapprich, S., Daniels, A.D., Farkas, Ö., Foresman, J.B., Ortiz, J.V., Cioslowski, J., Fox, D.J.: Gaussian 09. Gaussian, Inc., Wallingford (2009)
44. Lanucara, F., Crestoni, M.E., Chiavarino, B., Fornarini, S., Hernandez, O., Scuderi, D., Maitre, P.: Infrared spectroscopy of nucleotides in the gas phase 2. The protonated cyclic 3′,5′-adenosine monophosphate. RSC Adv. **3**, 12711–12720 (2013)
45. Yang, B., Wu, R.R., Polfer, N.C., Berden, G., Oomens, J., Rodgers, M.T.: IRMPD action spectroscopy of alkali metal cation–cytosine complexes: effects of alkali metal cation size on gas phase conformation. J. Am. Soc. Mass Spectrom. **24**, 1523–1533 (2013)
46. Wu, R.R., Yang, B., Berden, G., Oomens, J., Rodgers, M.T.: Gas-phase conformations and energetics of protonated 2′-deoxyguanosine and guanosine: IRMPD action spectroscopy and theoretical studies. J. Phys. Chem. B. **118**, 14774–14784 (2014)
47. Wu, R.R., Yang, B., Berden, G., Oomens, J., Rodgers, M.T.: Gas-phase conformations and energetics of protonated 2′-deoxyadenosine and adenosine: IRMPD action spectroscopy and theoretical studies. J. Phys. Chem. B. **119**, 2795–2805 (2015)
48. Wu, R.R., Yang, B., Frieler, C.E., Berden, G., Oomens, J., Rodgers, M.T.: Diverse mixtures of 2,4-dihydroxy tautomers and O4 protonated conformers of uridine and 2′-deoxyuridine coexist in the gas phase. Phys. Chem. Chem. Phys. **17**, 25978–25988 (2015)
49. Wu, R.R., Yang, B., Frieler, C.E., Berden, G., Oomens, J., Rodgers, M.T.: 2,4-Dihydroxy and O2 protonated tautomers of dThd and Thd coexist in the gas phase: methylation alters protonation preferences versus dUrd and Urd. J. Am. Soc. Mass Spectrom. **27**, 410–421 (2016)
50. Wu, R.R., He, C.C., Hamlow, L.A., Nei, Y.W., Berden, G., Oomens, J., Rodgers, M.T.: Protonation induces base rotation of purine nucleotides pdGuo and pGuo. Phys. Chem. Chem. Phys. **18**, 15081–15090 (2016)
51. Wu, R.R., He, C.C., Hamlow, L.A., Nei, Y.W., Berden, G., Oomens, J., Rodgers, M.T.: N3 protonation induces base rotation of 2′-deoxyadenosine-5′-monophosphate and adenosine-5′-monophosphate. J. Phys. Chem. B. **120**, 4616–4624 (2016)
52. Wu, R.R., Hamlow, L.A., He, C.C., Nei, Y.W., Berden, G., Oomens, J., Rodgers, M.T.: The intrinsic basicity of the phosphate backbone exceeds that of uracil and thymine residues: protonation of the phosphate moiety is preferred over the nucleobase for pdThd and pUrd. Phys. Chem. Chem. Phys. **19**, 30351–30361 (2017)
53. Wu, R.R., Chen, Y., Rodgers, M.T.: Mechanisms and energetics for N-glycosidic bond cleavage of protonated 2′-deoxyguanosine and guanosine. Phys. Chem. Chem. Phys. **18**, 2968–2980 (2016)
54. Wu, R.R., Rodgers, M.T.: Mechanisms and energetics for N-glycosidic bond cleavage of protonated adenine nucleosides: N3 protonation induces base rotation and enhances N-glycosidic bond stability. Phys. Chem. Chem. Phys. **18**, 16021–16032 (2016)
55. Wu, R.R., Rodgers, M.T.: Tautomerization lowers the activation barriers for N-glycosidic bond cleavage of protonated uridine and 2′-deoxyuridine. Phys. Chem. Chem. Phys. **18**, 24451–24459 (2016)
56. Wu, R.R., Rodgers, M.T.: O2 protonation controls threshold behavior for N-glycosidic bond cleavage of protonated cytosine nucleosides. J. Phys. Chem. B. **120**, 4803–4811 (2016)
57. Altona, C., Sundaralingam, M.: Conformational-analysis of sugar ring in nucleosides and nucleotides: new description using concept of pseudorotation. J. Am. Chem. Soc. **94**, 8205–8212 (1972)
58. Parneix, P., Basire, M., Calvo, F.: Accurate modeling of infrared multiple photon dissociation spectra: the dynamical role of anharmonicities. J. Phys. Chem. A. **117**, 3954–3959 (2013)
59. Scott, A.P., Radom, L.: Harmonic vibrational frequencies: an evaluation of Hartree−Fock, Møller−Plesset, quadratic configuration interaction, density functional theory, and semiempirical scale factors. J. Phys. Chem. **100**, 16502–16513 (1996)
60. Chiavarino, B., Crestoni, M.E., Fornarini, S., Lanucara, F., Lemaire, J., Maitre, P., Scuderi, D.: Infrared spectroscopy of isolated nucleotides. 1. The cyclic 3′,5′-adenosine monophosphate anion. Int. J. Mass Spectrom. **270**, 111–117 (2008)
61. Martens, J.K., Grzetic, J., Berden, G., Oomens, J.: Gas-phase conformations of small polyprolines and their fragment ions by IRMPD spectroscopy. Int. J. Mass Spectrom. **377**, 179–187 (2015)
62. Sediki, A., Snoek, L.C., Gaigeot, M.-P.: N–H^+ vibrational anharmonicities directly revealed from DFT-based molecular dynamics simulations on the $Ala7H^+$ protonated peptide. Int. J. Mass Spectrom. **308**, 281–288 (2011)
63. Yacovitch, T.I., Heine, N., Brieger, C., Wende, T., Hock, C., Neumark, D.M., Asmis, K.R.: Vibrational spectroscopy of bisulfate/sulfuric acid/water clusters: structure, stability, and infrared multiple-photon dissociation intensities. J. Phys. Chem. A. **117**, 7081–7090 (2013)